Physicochem. Probl. Miner. Process. 53(2), 2017, 829−845

www.minproc.pwr.wroc.pl/journal/

Physicochemical Problems of Mineral Processing

ISSN 1643-1049 (print)
ISSN 2084-4735 (online)

Received December 1, 2016; reviewed; accepted February 27, 2017

Preparation of activated bentonite and its adsorption behavior on oil-soluble green pigment

Renji Zheng, Huimin Gao, Zijie Ren, Duidui Cen, Zhijie Chen

School of Resources and Environmental Engineering, Wuhan University of Technology, Wuhan 430070, China. Corresponding author: gaohuimin1958@126.com (Huimin Gao)

Abstract: The present research work focuses on effective preparation of activated bentonite (AB) and its application in removal of oil-soluble green pigment (OSGP) from either vegetable oils or food-processing wastewater. Mono-factor experiments were carried out to explore the effects of operation factors in preparation of AB. The parameters investigated were the effect of contact time, adsorbent dosage, initial OSGP concentration and temperature. The chemical composition, crystalline phases, microstructure and functional groups of prepared AB were characterized and evaluated by X-ray fluorescence (XRF), X-ray diffraction (XRD), scanning electron microscopy (SEM) and Fourier transform infrared spectroscopy (FT-IR), respectively. The adsorption kinetics and equilibrium isotherms were studied, finding that the adsorption process fitted better with the pseudo-second-order model and the Freundlich isotherm equation. In addition, thermodynamic parameters, such as standard the Gibbs free energy ($\Delta G°$), standard enthalpy ($\Delta H°$) and standard entropy ($\Delta S°$) were also calculated, indicating that adsorption was spontaneous and endothermic. The findings of this investigation suggest that AB prepared through microwave activation as a cheap adsorbent holds great potential to remove oil-soluble green pigment in the wastewater treatment process.

Keywords: *activated bentonite, acid activation, microwave heating, oil-soluble green pigment, adsorption*

Introduction

As it is known, vegetable oils contain many kinds of pigments, including chlorophylls, carotenoids, xanthophylls and their derivatives, among them carotenoids and chlorophylls are found as the main pigments (Park and Ming, 2004; Wu and Li, 2009; Pohndorf et al., 2016). The existence of pigments in vegetable oils or other edible oils would cause many damages. The crude oils without either purifying or bleaching exhibit lower application value than refined ones and they may decompose into pheophytins by heat treatment, making the oil an opaque and dark color, especially for the chlorophylls within (Pohndorf et al., 2016; Sabah, 2007). Moreover, pigments in food-processing wastewater from the food oil industry, just like pigment effluents,

http://dx.doi.org/10.5277/ppmp170213

cause fearful environmental pollution. Pigments or pigment wastewaters have been a major concern due to their adverse effect on many forms of life, as well as grave fears for toxicological and esthetical reasons (Ravikumar et al., 2005; Zhao et al., 2012). Some solutions to the predicament mentioned above have become a necessity. With regard to treatment for pigment wastewater, biological process (Ledakowicz et al., 2001), oxidation (Lucas and Peres, 2006), chemical coagulation-flocculation (Moghaddama et al., 2010), membrane-based separation (Chakraborty et al., 2003; Purkait et al., 2006) and adsorption have been applied. Adsorption is considered to be a superior way to treat pigment effluents in terms of its low cost, high efficiency, easy handling, wide variety of adsorbents and high stability toward the adsorbents (Tan et al., 2008; Wu et al., 2008; Nandi et al., 2009; Yu and Fugetsu, 2010). Activated clays, activated carbon and silica-based products are adsorbents commonly used in the adsorptive bleaching process of vegetable oils, as described in previous reports (Bayrak, 2003; Caglayan et al., 2005; Liu et al., 2008; Su et al., 2013; Silva et al., 2013). However, only a few attempts have been focused on the influence of surface activity clays prepared with microwave activation, as well as the adsorption behavior of pigments from their model oil solutions at low temperature 25-45 °C.

In previous studies, the common method used in preparation of activated bentonite was either water-bath heating or hydrothermal process with acids (Oladipo and Gazi, 2014), which needed a long reaction time and was of low-efficiency. The use of microwave radiation in activation of clays offers advantages over conventional methods, including a higher heating rate in a shorter time, due to its volumetric heating (Korichi et al., 2012). To the best of our knowledge, more attention has been paid to preparation of activated clays using microwave activation.

Therefore, the objective of this study was to research effective preparation of AB through microwave heating. The operation factors of this process were studied in details. In addition, the characteristics of clay samples were estimated and evaluated with the use of XRF, XRD, FT-IR and SEM. Batch adsorption experiments, adsorption kinetics and equilibrium isotherms for OSGP removal were simulated. The effect of temperature on the adsorption behavior was further studied. Moreover, thermodynamic parameters such as the standard Gibbs free energy ($\Delta G°$), standard enthalpy ($\Delta H°$) and standard entropy ($\Delta S°$) were calculated.

Experimental

Materials

Activated bentonite used for adsorption experiments was obtained after microwave activation of preliminary beneficiation of raw bentonite (PBRB), which was achieved from the Huludao bentonite deposit in Liaoning Province, China. The oil-soluble green pigment (OSGP) was purchased from Kunshan Wanfukai Chemical Co., LTD., China, and was used without further processing. Figure 1 shows the chemical structure of chlorophyll-a, the main component of OSGP. Chlorophyll-a is mainly made up of

porphyrin and phytol, and the former makes it green, while the latter makes it hydrophobic.

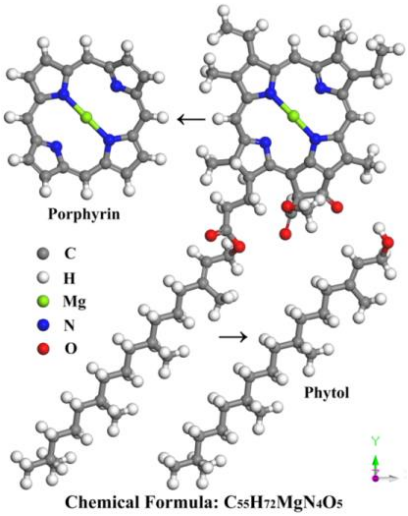

Fig. 1. Chemical structure of chlorophyll-a

Adsorbent preparation

In order to obtain PBRB, raw bentonite was ground into the powder form and sieved by sieve size of 45 μm. Sieved bentonite was washed with distilled water in order to remove the dust and other water soluble particles, and dried. Then, 25 g of PBRB powder was transferred to a quartz conical flask with particular concentration of sulfuric acid (H_2SO_4). The mixture was stirred and heated in a microwave oven under certain radiation power and activation time. Finally, the bentonite slurry was washed with distilled water until pH was 6–7, then dried in oven and stored for adsorption.

Adsorption experiments

For adsorption experiments, desired concentration and dosage of OSGP and adsorbent were transferred into a 50 cm^3 quartz conical flask, and shaken within define time, in temperature controlled by water bath shaker (SHA-BA, XINBAO, Jintan, China). The solid phase was separated from the solution using high-speed centrifuge (H2050R-1, CENCE Instruments Co., LTD., Hunan, China). Then, the absorbance of the residual OSGP in supernatant was measured at 422 nm, using a UV-Vis spectrophotometer (A-360, AOE Instruments Co., LTD., Shanghai, China) (Fig. 2).

The concentration of the residual OSGP was determined using the linear regression equation ($y = 1.85 \cdot 10^{-4}x + 0.034$, R^2=0.9994) obtained by plotting a calibration curve for OSGP over a concentrations range. The percentage removal of pigment was calculated using the following equation:

$$\% \text{ removal} = \frac{C_0 - C_t}{C_0} \times 100 \quad (1)$$

where, C_0 and C_t are the initial and at time t concentrations (mg/dm^3) of OSGP, respectively. The amount of adsorbed OSGP at equilibrium q_e (mg/g) was calculated using equation:

$$q_e = \frac{(C_0 - C_e)V}{m} \quad (2)$$

where, C_e is the equilibrium concentration of OSGP solutions (mg/dm^3), V is the volume of pigment solution (dm^3), m is the mass of adsorbent (g).

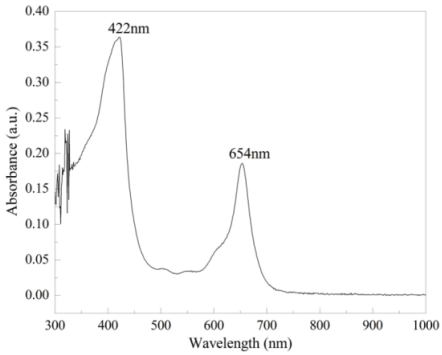

Fig. 2. UV-Vis absorption spectrum of OSGP

Analytical methods

The activity degree (mmol/kg) and decolorization ratio (%) were used to evaluate properties of AB prepared according to stipulation of Chinese standard (HG/T2569-2007). The chemical and phase composition of sample were determined by XRF (Axios advanced, PAN Alytical B.V., Netherlands) and XRD (D/Max-IIIA, RIGAKU, Japan) with monochromatic Cu Kα radiation, at an angle range of 3-70° and a rate of 0.02°/s. For the FT-IR analysis, adsorbent samples with OSGP adsorbed were dried at 60 ℃ for the sake of dislodging water within. FT-IR spectra were collected using a Nicolet spectrophotometer (IS-10, US). In order to characterize the surface morphology (to observe the clay frustules morphology of AB) and fundamental physical properties of the adsorbent, the scanning electron microscopy (JSM-5610LV, JEOL Ltd., Japan) with an accelerating voltage of 20 kV was applied.

Results and discussion

Effects of operation factors in preparation of activated bentonite

Mono-factor experiments were carried out to investigate the effects of the operation factors in preparation of Activated bentonite through microwave heating, including the

sulfuric acid (H_2SO_4) dosage, microwave power, liquid-to-solid ratio and activation time. Figure 3 shows the effect of operation factors on the activity degree and decolorization ratio of activated bentonite (AB). As shown in Fig. 3a, both parameters increased faster at low dosage of H_2SO_4 and almost reached equilibrium of 175 mmol/kg and 87.2% when the dosage of H_2SO_4 was 10%. No significant augment with further increase of H_2SO_4 was observed. An appropriate acid dosage could provide the sufficient hydrogen concentration for replacing interlayer cations such as Ca^{2+}, Na^{+}, K^{+} and Mg^{2+} of the clay sample, resulting in more reactive sites situated along the edges of the clay platelets (Mckinley et al., 1995; Korichi et al., 2009). Therefore, 10% of acid addition was chosen as the suitable dosage for further study.

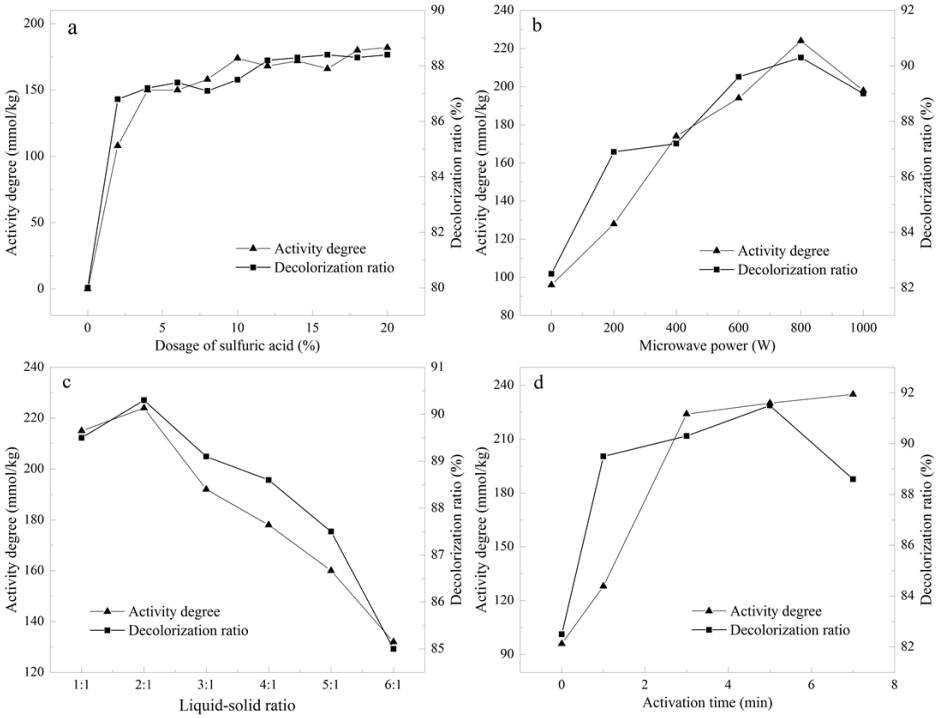

Fig. 3. Effects of operation parameters on activity degree and decolorization ratio of activated bentonite: (a) dose of H_2SO_4: microwave power = 350 W, liquid-solid ratio = 2:1, activation time = 3 min; (b) microwave power: acid dosage = 10%, liquid-solid ratio = 2:1, activation time = 3 min; (c) liquid-solid ratio: acid dosage = 10%, microwave power = 800 W, activation time = 3 min; (d) activation time: acid dosage = 10%, microwave power = 800 W, liquid-solid ratio = 2:1)

Figure 3b shows the influence of the microwave power on sample properties. It is evident that the activity degree and decolorization ratio of AB increased as the microwave power strengthened and both of them almost reached the maximum when it was 800 W. The properties of AB declined rapidly when the microwave power exceeded 800 W, mainly due to the structural collapse of clay during drastic

microwave heating. Similar behavior was also observed for the acid treatment of a bentonite from Algeria (Korichi et al., 2009) and Brazil (Foletto et al., 2013) under microwave radiation. A suitable microwave power could provide a stable and uniform activation atmosphere, promoting the activation rate of sample in the microwave oven, and therefore 800 W was chosen for further study.

The liquid-to-solid ratio (Fig. 3c) was considered as one of the important parameters in preparation of AB. The activity degree and decolorization ratio of AB reached the maximum at liquid-to-solid ratio of 2:1 and decreased continuously when it exceeded 2:1. The main reason was that the high liquid-to-solid ratio resulted in higher moisture content in the sample, which restrained the heating and activation of sample, and downgraded the properties of AB. Too low liquid-to-solid ratio disabled a sufficient heat-transfer medium for the activation reaction of sample in the microwave oven.

An appropriate activation time can not only control the whole process in preparation of AB, but also should determine the activation efficiency. The Experimental measurement of activation time (Fig. 3d) displayed that the activity degree of AB augmented gradually with increase of activation time from 0 to 7 min. By contrast, the decolorization ratio of AB reached the maximum when the activation time was 5 min, and then decreased probably due to disaggregation of clay structure, the similar phenomenon caused by excessive microwave heating. Comprehensively, 5 min was chosen as the optimal activation time, and the activity degree and decolorization ratio of AB were 230 mmol/kg and 91.5%, respectively.

Characterization of activated bentonite

Table 1 lists the chemical composition of PBRB and AB samples treated under optimum condition. The content of SiO_2 increased feebly mainly due to dissolution of interlayer cations by hydratation. The ion dissolving-out ratio of different cations of AB is further shown in Fig. 4. As compared to PBRB, interlayer cations such as Ca^{2+}, Na^+, K^+, Mg^{2+} and Fe^{3+} of the clay sample dissolved out to varying degrees during acid activation under microwave irradiation. The ion dissolving-out ratio of Ca^{2+} was even up to 48.98%.

Table 1. Chemical composition of preliminary beneficiation of raw bentonite (PBRB) and activated bentonite (AB)

Component	SiO_2	Al_2O_3	MgO	CaO	Fe_2O_3
PBRB (wt. %)	68.391	13.551	3.823	1.819	1.215
AB (wt. %)	69.072	13.272	3.421	0.928	1.116
Component	K_2O	Na_2O	TiO_2	P_2O_5	L.O.I.*
PBRB (wt. %)	0.461	0.195	0.132	0.165	10.159
AB (wt. %)	0.356	0.123	0.116	0.026	11.510

*Loss-on-ignition

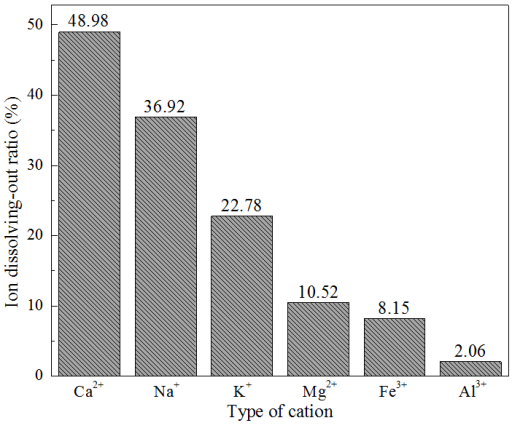

Fig. 4. Ion dissolving-out ratio of activated bentonite

The structural changes occurred in the clay material due to the acid treatment were studied using XRD. The XRD patterns of PBRB and AB activated with different dosages of H_2SO_4 are given in Fig. 5a. The main phase compositions of PBRB were montmorillonite, cristobalite and quartz. The *d* spacing of typical characteristic peak of the 001 plane (d_{001}) of montmorillonite was 16.744 Å (1.6744 nm), indicating that PBRB belongs to calcium bentonite and it tapered off from 16.744 to 14.337 Å (1.6744 to 1.4337 nm) with the H_2SO_4 dosage increasing from 0 to 30%. It reflected that the inner chemical structure of montmorillonite was destroyed through microwave heating with acid. Moreover, the diffraction intensity of the typical characteristic peak of the 001 plane of montmorillonite dropped rapidly, especially as the dosage of H_2SO_4 exceeded 10%. Generally, the 001 reflection appeared broad and weak after acid activation due to the partial destruction of the layered structure of montmorillonite (Pawar et al., 2016). Reduction in the intensity and increase in the width of the 001 peak indicated that the crystallinity of AB was considerably affected by acid activation. Therefore, 10% was demonstrated as a moderate dosage of H_2SO_4, which was also in accordance with the obtained experimental results (Fig. 3a).

As shown in Fig. 5b, the FT-IR spectra of AB activated with different dosages of H_2SO_4 present two distinct absorption bands in high frequencies: the absorption band at about 3620 cm^{-1} was related to the Al-O-H stretching vibration, and this at 3436 cm^{-1} reflected to the H-O-H stretching vibration of the interlayer water of montmorillonite. The H-O-H bending vibration of water was observed at 1640 cm^{-1} correspondingly. With increasing dosage of H_2SO_4 from 0 to 30%, the absorption band of Al-O-H stretching vibration of AB moved triflingly to the high frequencies from 3621 to 3637 cm^{-1}. The reason was the loss of hydroxyls in the montmorillonite structure during acid treatment, and formation of new weaker Si-OH and A1-OH bonds. This caused dehydroxylation, which made cations (Al^{3+}) weaker induction force for the electron cloud of O-H bond (Korichi et al., 2009; Korichi et al., 2012). A sharp absorption band at 1030 cm^{-1} was assigned to the asymmetric stretching

vibration of Si-O-Si bond of montmorillonite, and absorption bands at 1089, 795 and 469 cm^{-1} represented the asymmetric stretching, symmetric stretching and bending vibrations of Si-O-Si bond, respectively (Saidi et al., 2012). The band at 521 cm^{-1} indicated the coupled vibration of Si-O-M (M means cation) from octahedral site of montmorillonite, and the intensity tapered off due to continuous dissolution of cations from the octahedral sites during acid activation.

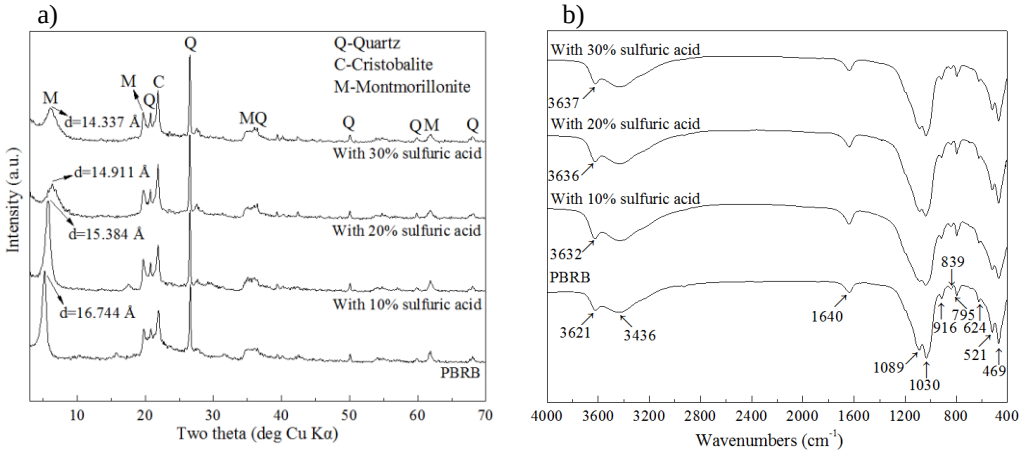

Fig. 5. XRD patterns (a) and FT-IR spectra (b) of PBRB and AB sample activated with different dosages of H_2SO_4

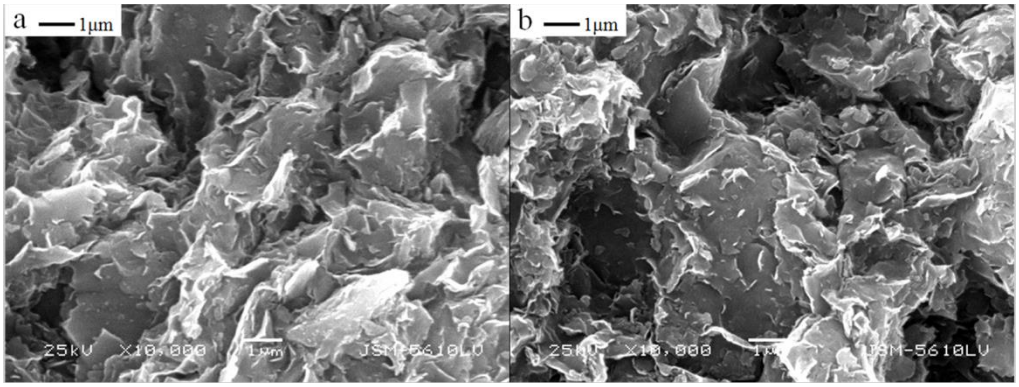

Fig. 6. SEM images of (a) PBRB and (b) AB samples

SEM images (Fig. 6) were made to probe the changes in the morphological features of PBRB and AB activated with H_2SO_4. The surface morphology of the PBRB was totally different from the acid treated sample. AB (Fig. 6b) possessed larger pores between the particles than PBRB (Fig. 6a) because of dissolving impurities and opening the edges of the platelets in sample during acid treatment (Korichi et al., 2009), which made it more active than PBRB. In addition, the PBRB appeared to be

highly compact, and the inter-particle pores were smaller than those in the AB sample. The micrograph of AB indicated disaggregation and decrease in the size of the clay structure during acid treatment.

Batch adsorption tests

A moderate adsorbent dosage cannot only enable good removal of OSGP, but also be economically viable. The influence of adsorbent concentration on OSGP removal by AB and PBRB is shown in Fig. 7. The surface area or the number of active sites for AB was naturally increased for the sorption reaction with an increase in the amount of adsorbent. Therefore, the percentage removal of pigment ascended as the adsorbent concentration increased from 20 to 60 g/dm^3, and almost reached equilibrium at 35 g/dm^3. As compared to PBRB, AB presented both higher percentage removal of OSGP and adsorption capacity because of forming new reactive sites after acid treatment. The suitable adsorbent concentration of 35 g/dm^3, at which OSGP removal was 63.74%, was chosen for further mono-factor experiments.

In order to estimate the equilibrium contact time for adsorption of OSGP onto AB and PBRB, the adsorption study was carried out at different time interval ranges from 0 to 220 min, under certain conditions (Fig. 8). OSGP was rapidly adsorbed by AB and PBRB with increasing the contact time up to 40 min, and then became constant as the contact time went by. The adsorption rate was faster at the beginning because the OSGP molecules were adsorbed by the exterior surface at the early stage, and then after its saturation, adsorbed by the interior surface of the adsorbent (Amin, 2009). For further study 40 min was selected as the equilibrium time.

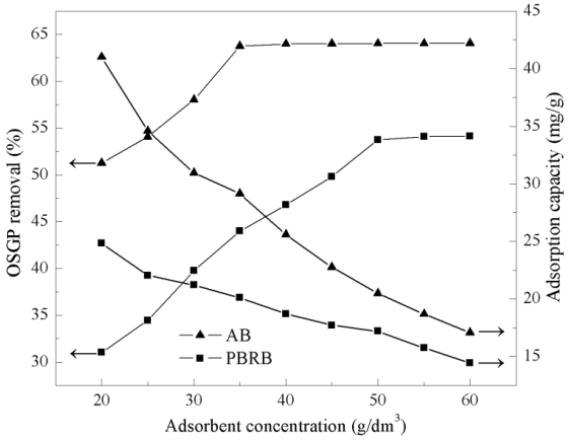

Fig. 7. Effect of adsorbent concentration on OSGP removal by AB and PBRB (contact time = 120 min, pigment concentration = 1600 mg/dm^3, temperature = 298 K)

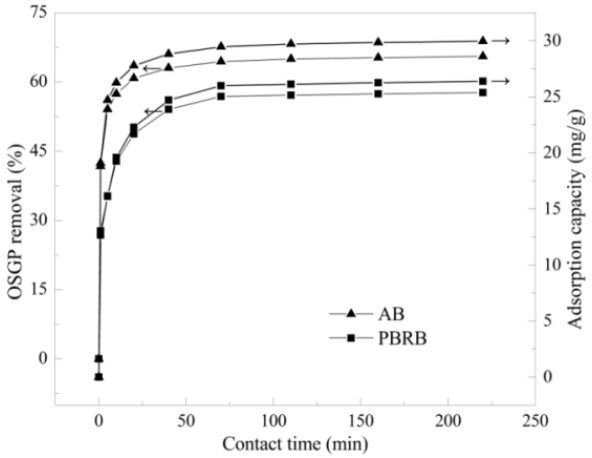

Fig. 8. Effect of contact time on OSGP removal (dose of AB = 35 g/dm^3, dose of PBRB = 50 g/dm^3, pigment concentration = 1600 mg/dm^3, temperature = 298 K)

The effect of initial concentration of OSGP and adsorption temperature on the amount of adsorbed pigment onto AB (Fig. 9) were discussed in details. The amount of adsorbed pigment increased with increasing its concentration in the range of 800-4800 mg/dm^3, at the same temperature. This amount can be higher with higher concentration of OSGP at the same amount of adsorbent. It resulted from an increase in mass transfer driving force due to concentration gradient developed between the bulk solution and surface of the adsorbent (Purkait et al., 2006). In addition, adsorption of OSGP onto AB ascended as the solution temperature increased, from which it can be speculated that the adsorption process was endothermic and spontaneous.

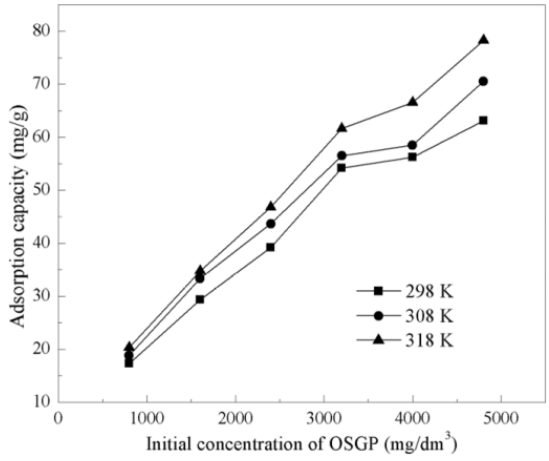

Fig. 9. Effect of initial concentration of OSGP and temperature on amount of adsorbed pigment onto AB (dose of AB = 35 g/dm^3, contact time = 40 min)

Adsorption kinetics, isotherms and thermodynamics

Adsorption kinetics

In order to investigate the mechanism of the adsorption process of OSGP onto AB, kinetics data were checked through the pseudo-first-order and pseudo-second-order models reported by Ho and McKay (1999):

$$\ln(q_e - q_t) = \ln q_e - k_1 t \tag{3}$$

$$\frac{1}{(q_e - q_t)} = k_2 t + \frac{1}{q_e} \tag{4}$$

where k_1 (min^{-1}) is the pseudo-first-order rate constant, k_2 ($g \cdot mg^{-1} \cdot min^{-1}$) is the equilibrium rate constant of pseudo-second-order kinetic model, q_e and q_t are the amounts of OSGP adsorbed at equilibrium (mg/g) and time t (min). The slope of plot of $\ln(q_e - q_t)$ vs. t (Fig. 10a) was used to calculate q_e and k_1, which are listed in Table 2. The values of $1/(q_e - q_t)$ were linearly correlated with t (Fig. 10b) and the plot of $1/(q_e - q_t)$ against t gave a linear relationship from which the values of k_2 were determined based on the slope of the plot.

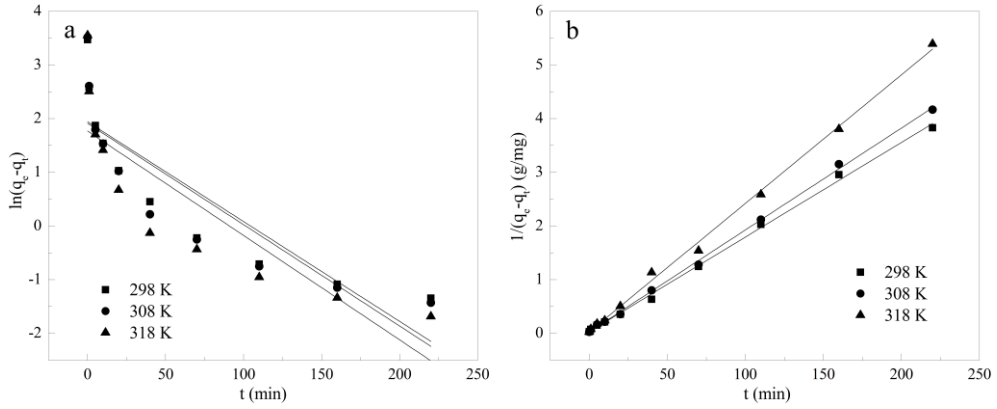

Fig. 10. Pseudo-first (a) and pseudo-second (b) order kinetic models for adsorption of OSGP onto AB

The comparison of pseudo-first-order and pseudo-second-order (Table 2) kinetic parameters revealed that the kinetic study followed pseudo-second-order kinetics model better because of its high regression coefficient value (R^2). Moreover, the theoretical amount of pigment adsorbed was found to be very close to the experimental results (Fig. 8). The equilibrium amount of pigment adsorbed q_e (31.47 mg/g) at 298 K (25 °C) in theory coincided with the real amount of pigment adsorbed (30.58 mg/g) obtained in the experiment. In addition, the rate constant (k_2) aggrandized with the increase of temperature, which confirmed the endothermic nature of the adsorption process.

Table 2. Kinetic parameters for adsorption of OSGP on AB

T (K)	Pseudo-first-order			Pseudo-second-order		
	q_e (mg/g)	k_1 (min^{-2})	R^2	q_e (mg/g)	k_2 (g/mg min)	R^2
298	6.9807	1.860×10^{-2}	0.7704	31.4683	1.763×10^{-2}	0.9980
308	6.7797	1.889×10^{-2}	0.7587	33.7211	1.898×10^{-2}	0.9990
318	5.8695	1.945×10^{-2}	0.7332	34.9650	2.394×10^{-2}	0.9977

Equilibrium isotherms

Adsorption isotherms are important for description of interaction between adsorbed molecules and adsorbent surface, and are basic requirements for design of adsorption systems (Amin, 2009; Zhao et al., 2012). The Langmuir and Freundlich adsorption isotherms were used in order to interpret the data of adsorption of OGSP onto AB, based on the results presented in Fig. 9. Isotherm equations are given as (Periasamy and Namasivayam, 1995):

$$\frac{C_e}{q_e} = \frac{1}{k_L q_m} + \frac{C_e}{q_m} \tag{5}$$

$$\ln q_e = \ln k_F + \frac{\ln c_e}{n} \tag{6}$$

where q_m (mg/g) and k_L (dm^3/mg) are Langmuir isotherm coefficients. The value of q_m represents the maximum adsorption capacity, k_F [(mg/g)(dm^3/mg)$^{1/n}$] and n are Freundlich constants. The Langmuir (C_e/q_e vs. C_e) plots and linear plots of Freundlich ($\ln q_e$ vs. $\ln C_e$) for the adsorption of OGSP onto AB, at different temperatures, were simulated (Fig. 11) according to Eq. (5-6), and a proper parameters were calculated.

Based on isotherms model results (Table 3), the correlation coefficients (R^2) of the linear form of the Freundlich model were noted higher than that of the Langmuir model at each temperature. It means that the adsorption process of OSGP onto AB follows the Freundlich model better, the adsorption has multilayer nature.

Table 3. Isotherm parameters for the adsorption of OSGP onto AB

T (K)	Langmuir isotherm			Freundlich isotherm		
	k_L (dm^3/mg)	q_m (mg/g)	R^2	k_F [(mg/g)(dm^3/mg)$^{1/n}$]	1/n	R^2
298	1.071×10^{-3}	84.246	0.9500	1.148	0.5154	0.9745
308	1.603×10^{-3}	83.313	0.9562	2.044	0.4548	0.9843
318	1.858×10^{-3}	92.439	0.9389	2.967	0.4242	0.9851

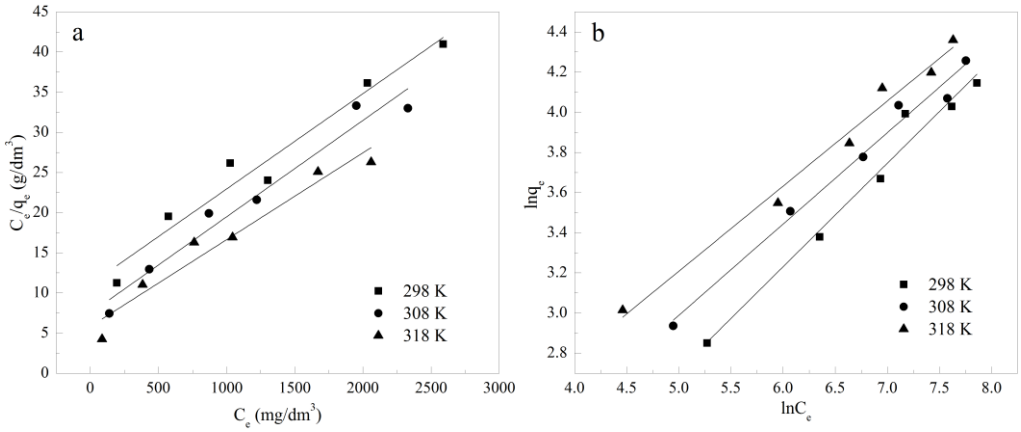

Fig. 11. Langmuir (a) and Freundlich (b) isotherms for adsorption of OSGP onto AB

Thermodynamic study

The thermodynamic parameters provide in-depth information about the energetic changes associated with the adsorption process (Sharma and Das, 2014). Therefore, thermodynamic parameters such as the enthalpy (*ΔH*°), free energy change or adsorption energy (*ΔG*°) and entropy (*ΔS*°) were investigated using following equations (Chowdhury et al., 2011):

$$\Delta G^0 = -RT \ln K_c \tag{7}$$

$$\Delta G^0 = \Delta H^0 - T\Delta S^0 \tag{8}$$

where K_c is the distribution coefficient determined as:

$$K_c = \frac{C_a}{C_e} \tag{9}$$

where C_a is the equilibrium pigment concentration on the adsorbent (mg/dm^3), C_e is the equilibrium pigment concentration in the solution (mg/dm^3), T is temperature (K), and R is the gas constant (8.314 J/mol^{-1}·K^{-1}). The Gibbs free energies (Δ*G*°) for adsorption of OSGP onto AB obtained at all temperatures are listed in Table 4. The enthalpy (Δ*H*°) and entropy (Δ*S*°) were determined from the slope and intercept of the plot of Δ*G*° vs. *T* (figure not shown) and are also tabulated. The results presented in Table 4 revealed that the adsorption process had the spontaneous nature as indicated by the negative values of Δ*G*°. Physical adsorption could have played an important role in OSGP uptake for the Δ*G*° values in the range of –20 to 0 KJ/mol (Li et al., 2011). The positive value of Δ*H*° revealed endothermic adsorption and this was in the agreement with the expected higher negative values of Δ*G*° at higher temperatures. The positive value of Δ*S*° suggested increased randomness at the solid/solution interface during adsorption (Acemioğlu, 2004).

Table 4. Thermodynamic parameters for adsorption of OSGP onto AB

T (K)	$\Delta G°$ (KJ/mol)	$\Delta S°$ (J mol^{-1}·K^{-1})	$\Delta H°$ (KJ/mol)
298	-2.1388		
308	-2.6343	47.2539	11.9352
318	-3.0839		

Adsorption mechanism

FT-IR spectroscopy has become an important tool for analyzing the adsorption mechanism through the changes in the bands assigned to the characteristic functional groups present on the adsorbent surface. The FT-IR spectra of AB, OSGP and AB recorded after the OSGP adsorption are presented (Fig. 12), while the FT-IR spectra of AB sample were described in details in Fig. 5b. For OSGP, the strong absorption bands at about 2925 cm^{-1} and 2851 cm^{-1} were assigned to the asymmetric stretching and symmetric stretching vibrations of –CH_2 group. Correspondingly, the bands at about 1464, 1375 and 726 cm^{-1} represented the bending, twisting and rocking vibration of –CH_2 group, respectively. The strong absorption band at about 1744 cm^{-1} reflected the stretching vibration of C=O group. There were three weak absorption bands at about 1097, 1163 and 1238 cm^{-1} reflecting the vibration characteristics for porphyrin group in chlorophyll-a (Fig. 1). The FT-IR spectrum of the sample after adsorption (AB + OSGP) was composed with several new absorption bands at about 2928, 2855, 1744 and 1458 cm^{-1}, which indicated physical adsorption. Moreover, there was no prominent change in the spectrum of AB after OSGP adsorption except the mention above bands. Moreover, the weakening of the bands at 3629, 3448, 1647, 1086 and 1039 cm^{-1} compared with spectrum of AB, confirmed that chemical adsorption was insignificant and negligible during OSGP uptake by AB.

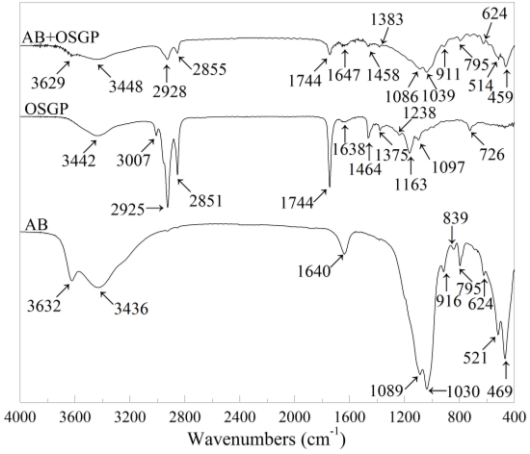

Fig. 12. FT-IR spectra of AB, OSGP and AB + OSGP samples

Conclusions

This study explored microwave activation as an effective method for preparation of activated bentonite (AB). AB prepared had higher affinity to adsorb OSGP than BPRB due to the more acid reactive sites forming by acid activation. The adsorption experiments showed that the maximum amount of OSGP adsorbed onto AB was about 30.58 mg/g. The adsorption process of OSGP fitted better with the pseudo-second-order kinetic model and the equilibrium data were described better with the Freundlich isotherm model, which indicated a heterogeneous surface binding during the adsorption process. In addition, determination of the thermodynamic parameters ($\Delta G°$, $\Delta H°$ and $\Delta S°$) revealed the spontaneous and endothermic nature of the adsorption process, and the positive value of $\Delta S°$ suggested increasing randomness at the solid/solution interface during the adsorption process. Physical adsorption was proposed to play an important role according to the consequences of thermodynamic parameters and FT-IR analysis. Taking into consideration all the results, it can be concluded that the microwave activated bentonite can be an alternative adsorbent used for pigment removal in wastewater treatment processes.

Acknowledgments

This work was financially supported by the Essential Science Indicators Promotion Project of Wuhan University of Technology (451/35400694), China. The authors are thankful to Hubei Key Laboratory of Mineral Resources Processing and Environment, Wuhan University of Technology for providing experimental facilities they needed and showing supports in carrying out this work.

References

AMIN, N. K., 2009, *Removal of direct blue-106 pigment from aqueous solution using new activated carbons developed from pomegranate peel: adsorption equilibrium and kinetics*, J. Hazard. Mater. 165, 52-62.

ACEMIOĞLU, B., 2004, *Adsorption of Congo red from aqueous solution onto calcium-rich fly ash*, J. Colloid Interf. Sci. 274, 371-379.

BAYRAK, Y., 2003, *Adsorption isotherms in bleaching hazelnut oil*, J. Am. Oil Chem. Soc. 80, 1143-1146.

CAGLAYAN, M. O., KAFA, S., YIGIT, N., 2005, *Al-pillared clay for cottonseed oil bleaching: an optimization study*, J. Am. Oil Chem. Soc. 82, 599-602.

CHOWDHURY, S., MISHRA, R., SAHA, P., KUSHWAHA, P., 2011, *Adsorption thermodynamics, kinetics and isosteric heat of adsorption of malachite green onto chemically modified rice husk*, Desalination 265, 159-168.

CHAKRABORTY, S., PURKAIT, M. K., DASGUPTA, S., DE, S., BASU, J. K., 2003, *Nanofiltration of textile plant effluent for color removal and reduction in COD*, Sep. Purif. Technol. 31, 141-151.

FOLETTO, E. L., PAZ, D. S., GUNDEL, A., 2013, *Acid-activation assisted by microwave of a Brazilian bentonite and its activity in the bleaching of soybean oil*, Appl. Clay Sci. 83-84, 63-67.

HO, Y. S., MCKAY, G., 1999, *Pseudo-second order model for sorption processes*, Process Biochem. 34, 451-465.

HG/T 2569-2007, 2007, *Acticated bentonite*, Chemical industry standard of China. (in Chinese)

KORICHI, S., ELIAS, A. L., MEFTI, A., 2009, *Characterization of smectite after acid activation with microwave irradiation*, Appl. Clay Sci. 42, 432-438.

KORICHI, S., ELIAS, A. L., MEFTI, A., BENSMAILI, A., 2012, *The effect of microwave irradiation and conventional acid activation on the textural properties of smectite: Comparative study*, Appl. Clay Sci. 59-60, 76-83.

LI, Y., DU, Q., LIU, T., QI, Y., ZHANG, P., WANG, Z., XIA, Y., 2011, *Preparation of activated carbon from Enteromorpha prolifera and its use on cationic red X-GRL removal*, Appl. Surf. Sci. 257, 10621-10627.

LIU, Y., HUANG, J., WANG, X., 2008, *Adsorption isotherms for bleaching soybean oil with activated attapulgite*, J. Am. Oil Chem. Soc. 85, 979-984.

LEDAKOWICZ, S., SOLECKA, M., ZYLLA, R., 2001, *Biodegradation, decolourisation and detoxification of textile wastewater enhanced by advanced oxidation processes*, J. Biotechnol. 89, 175-184.

LUCAS, M. S., PERES, J. A., 2006, *Decolorization of the azo pigment Reactive Black 5 by Fenton and photo-Fenton oxidation*, Pigments Pigments, 71, 236-244.

MCKINLEY, J. P., ZACHARA, J. M., SMITH, S. C., TURNER, G. D., 1995, *The influence of uranyl hydrolysis and multiple site-binding reactions on adsorption of U(VI) to montmorillonite*, Clay. Clay Miner. 43, 586-598.

MOGHADDAM, S. S., MOGHADDAM, M. A., ARAMI, M., 2010, *Coagulation/flocculation process for pigment removal using sludge from water treatment plant: optimization through response surface methodology*, J. Hazard. Mater. 175, 651-657.

NANDI, B. K., GOSWAMI, A., PURKAIT, M. K., 2009, *Adsorption characteristics of brilliant green pigment on kaolin*, J. Hazard. Mater. 161, 387-395.

OLADIPO, A. A., GAZI, M., 2014, *Enhanced removal of crystal violet by low cost alginate/acid activated bentonite composite beads: optimization and modelling using non-linear regression technique*, J. Water Process Eng. 2, 43-52.

POHNDORF, R. S., JR, T. R. S. C., PINTO, L. A. A., 2016, *Kinetics and thermodynamics adsorption of carotenoids and chlorophylls in rice bran oil bleaching*, J. Food Eng. 185, 9-16.

PAWAR, R. R., BAJAJ, H. C., LEE, S. M., 2016, *Activated bentonite as a low-cost adsorbent for the removal of Cu (II) and Pb (II) from aqueous solutions: Batch and column studies*, J. Ind. Eng. Chem. 34, 213-223.

PERIASAMY, K., NAMASIVAYAM, C., 1995, *Removal of nickel (II) from aqueous solution and nickel plating industry wastewater using an agricultural waste: peanut hulls*, Waste Manage. 15, 63-68.

PARK, E. Y., MING, H., 2004, *Oxidation of rapeseed oil in waste activated bleaching earth and its effect on riboflavin production in culture of Ashbya gossypii*, J. Biosci. Bioeng. 97, 59-64.

PURKAIT, M. K., DASGUPTA, S., DE, S., 2006, *Micellar enhanced ultrafiltration of eosin pigment using hexadecyl pyridinium chloride*, J. Hazard. Mater. 136, 972-977.

RAVIKUMAR, K., DEEBIKA, B., BALU, K., 2005, *Decolourization of aqueous pigment solutions by a novel adsorbent: application of statistical designs and surface plots for the optimization and regression analysis*, J. Hazard. Mater. 122, 75-83.

SABAH, E., 2007, *Decolorization of vegetable oils: Chlorophyll-a adsorption by acid-activated sepiolite*, J. Colloid Interf. Sci. 310, 1-7.

SU, D., XIAO, T., GU, D., CAO, Y., JIN, Y., ZHANG, W., WU, T., 2013, *Ultrasonic bleaching of rapeseed oil: effects of bleaching conditions and underlying mechanisms*, J. Food Eng. 117, 8-13.

SILVA, S. M., SAMPAIO, K. A., CERIANI, R., VERHé, R., STEVENS, C., DE GREYT, W., MEIRELLES, A. J., 2013, *Adsorption of carotenes and phosphorus from palm oil onto acid activated bleaching earth: Equilibrium, kinetics and thermodynamics*, J. Food Eng. 118, 341-349.

SAIDI, R., TLILI, A., FOURATI, A., AMMAR, N., OUNIS, A., JAMOUSSI, F., 2012, *Granulometric distribution of natural and flux calcined chert from Ypresian phosphatic series of Gafsa-Metlaoui basin compared to diatomite filter aid*, In IOP Conference Series: Materials Science and Engineering (Vol. 28, No. 1, p. 012027), IOP Publishing.

SHARMA, P., DAS, M. R., 2014, *Removal of a cationic pigment from aqueous solution using graphene oxide nanosheets: investigation of adsorption parameters*, J. Chem. Eng. Data 58, 151-158.

TAN, I. A. W., AHMAD, A. L., HAMEED, B. H., 2008, *Adsorption of basic pigment on high-surface-area activated carbon prepared from coconut husk: Equilibrium, kinetic and thermodynamic studies*, J. Hazard. Mater. 154, 337-346.

WU, Z., LI, C., 2009, *Kinetics and thermodynamics of β-carotene and chlorophyll adsorption onto acid-activated bentonite from Xinjiang in xylene solution*, J. Hazard. Mater. 171, 582-587.

WU, J. S., LIU, C. H., CHU, K. H., SUEN, S. Y., 2008, *Removal of cationic pigment methyl violet 2B from water by cation exchange membranes*, J. Membrane Sci. 309, 239-245.

YU, H., FUGETSU, B., 2010, *A novel adsorbent obtained by inserting carbon nanotubes into cavities of diatomite and applications for organic pigment elimination from contaminated water*, J. Hazard. Mater. 177, 138-145.

ZHAO, Y., XUE, Z., WANG, X., WANG, L., WANG, A., 2012, *Adsorption of congo red onto lignocellulose/montmorillonite nanocomposite*, J. Wuhan Univ. Technol. 27, 931-938.